AGU PUBLICATIONS

Global Biogeochemical Cycles

RESEARCH ARTICLE
10.1002/2014GB005034

Key Points:
- NEE relationships with enviroclimatic drivers inferred from atmospheric data
- NEE patterns tied to radiation (humidity) during growing (transition) season
- Biospheric model performance tied to dominant enviroclimatic drivers

Supporting Information:
- Figures S1–S5
- Table S1

Correspondence to:
Y. Fang,
yyfang@carnegiescience.edu

Citation:
Fang, Y., and A. M. Michalak (2015), Atmospheric observations inform CO_2 flux responses to enviroclimatic drivers, *Global Biogeochem. Cycles*, *29*, 555–566, doi:10.1002/2014GB005034.

Received 6 NOV 2014
Accepted 1 APR 2015
Accepted article online 7 APR 2015
Published online 12 MAY 2015

Atmospheric observations inform CO_2 flux responses to enviroclimatic drivers

Yuanyuan Fang[1] and Anna M. Michalak[1]

[1]Department of Global Ecology, Carnegie Institution for Science, Stanford, California, USA

Abstract Understanding the response of the terrestrial biospheric carbon cycle to variability in enviroclimatic drivers is critical for predicting climate-carbon interactions. Here we apply an atmospheric-inversion-based framework to assess the relationships between the spatiotemporal patterns of net ecosystem CO_2 exchange (NEE) and those of enviroclimatic drivers. We show that those relationships can be directly observed at $1° \times 1°$ 3-hourly resolution from atmospheric CO_2 measurements for four of seven large biomes in North America, namely, (i) boreal forests and taiga; (ii) temperate coniferous forests; (iii) temperate grasslands, savannas, and shrublands; and (iv) temperate broadleaf and mixed forests. We find that shortwave radiation plays a dominant role during the growing season over all four biomes. Specific humidity and precipitation also play key roles and are associated with decreased CO_2 uptake (or increased release). The explanatory power of specific humidity is especially strong during transition seasons, while that of precipitation appears during both the growing and dormant seasons. We further find that the ability of four prototypical terrestrial biospheric models (TBMs) to represent the spatiotemporal variability of NEE improves as the influence of radiation becomes more dominant, implying that TBMs have a better skill in representing the impact of radiation relative to other drivers. Even so, we show that TBMs underestimate the strength of the relationship to radiation and do not fully capture its seasonality. Furthermore, the TBMs appear to misrepresent the relationship to precipitation and specific humidity at the examined scales, with relationships that are not consistent in terms of sign, seasonality, or significance relative to observations. More broadly, we demonstrate the feasibility of directly probing relationships between NEE and enviroclimatic drivers at scales with no direct measurements of NEE, opening the door to the study of emergent processes across scales and to the evaluation of their scaling within TBMs.

1. Introduction

Relationships between enviroclimatic drivers and land-atmosphere carbon exchange can potentially inform the climate sensitivities of the land carbon sink and the environmental processes controlling this sink. Diagnosing, understanding, and correctly representing these relationships within terrestrial biospheric models (TBMs) is therefore critical for predicting the future dynamics of the global biogeochemical carbon cycle and its interaction with the Earth climate system [*Cox et al.*, 2013; *Piao et al.*, 2013; *Yi et al.*, 2010].

By examining the spatial and/or temporal variability of net ecosystem CO_2 exchange (NEE) and its covariance with enviroclimatic drivers, previous observation-based studies found that strong relationships exist between those drivers and NEE, and that those relationships vary substantially across spatiotemporal scales. Globally, for example, the interannual variability of the observed atmospheric CO_2 growth rate, which is representative of global land carbon uptake, has been shown to be correlated with the El Niño–Southern Oscillation index and tropical temperatures [*Cox et al.*, 2013; *Heimann and Reichstein*, 2008; *Wang et al.*, 2013; *X. Wang et al.*, 2014]. Hemispherically, the interannual variability in the satellite-derived atmospheric CO_2 growth rate shows a positive correlation with the boreal warm season surface temperature anomaly [*Schneising et al.*, 2014]. At much smaller spatial scales, where NEE can be quantified using the eddy covariance technique (i.e., ~1 km^2), the temporal variability of NEE has been shown to be predominately driven by enviroclimatic drivers including temperature, humidity, and precipitation on daily to seasonal scales [*Law et al.*, 2002; *Mueller et al.*, 2010; *Yadav et al.*, 2010]. For example, *Mueller et al.* [2010] found that linear relationships with a limited number of drivers can explain around 80% (90%) of the daily (monthly) NEE variability. Spatial patterns of CO_2 fluxes have also been found to be sensitive to enviroclimatic drivers, with the dominant drivers varying across regions [*Beer et al.*, 2010; *Yi et al.*, 2010; *Yu et al.*, 2013].

Relationships between NEE and enviroclimatic drivers diagnosed directly from the observed spatiotemporal variability of carbon fluxes can be used to evaluate process-based terrestrial biospheric models (TBMs) and

inform the further development of these models [e.g., *Piao et al*., 2013; *Wang et al*., 2013; *X. Wang et al*., 2014]. For example, by examining the responses of carbon fluxes to climate variability and atmospheric CO_2 trends from both TBMs and observations, *Piao et al*. [2013] found that TBMs tend to overestimate the sensitivity of net biome productivity to atmospheric CO_2 and precipitation and attributed these process-level biases to the lack of representation of nutrient limitation in the current generation of TBMs. By examining the interannual variability of the atmospheric CO_2 growth rate, *X. Wang et al*. [2014] found that TBMs do not reproduce the stronger responses of the atmospheric CO_2 growth rate to increased tropical temperatures during the past five decades, suggesting a potential limitation in the representation of the impact of drought on tropical ecosystems.

Improving the process-level representation of biogeochemical cycles requires a better understanding of key drivers across a full spectrum of spatiotemporal scales. Of particular interest are scales corresponding to typical resolutions of TBMs run for regional to continental analyses. *Fang et al*. [2014] used atmospheric CO_2 mixing ratio measurements to evaluate the spatiotemporal patterns of NEE at 3-hourly and $1° \times 1°$ resolution, as predicted by several TBMs. Results showed that TBMs face challenges in simulating spatiotemporal NEE variability at such scales, especially during transition seasons, indicating a need to better understand environmental processes controlling variability at these scales. In response to this need, we propose here the use of atmospheric CO_2 mixing ratio measurements to evaluate the ability of TBMs to represent relationships between the NEE spatiotemporal variability and major enviroclimatic drivers at these same scales. We term these "fine scales" in the discussion that follows, as they are near the high end of resolutions that have been examined within the context of regional atmospheric inverse modeling studies.

Our study is inspired by, and builds upon, a series of previous efforts. *Gourdji et al*. [2012] showed that environmental processes controlling the fine-scale spatiotemporal variability of NEE can be inferred from atmospheric CO_2 measurements collected from a limited number of towers in North America. Using a larger observational data set, *Fang et al*. [2014] found that atmospheric CO_2 data can inform the performance of TBMs in simulating the fine-scale spatiotemporal variability of NEE within specific biomes and months. Furthermore, *Huntzinger et al*. [2011] used TBM predictions of NEE to compare relationships between enviroclimatic drivers and NEE as predicted by different models. Together, these earlier studies suggest that it is possible to build a framework for using atmospheric CO_2 measurements to evaluate TBMs based on how they simulate relationships between fine-scale NEE spatiotemporal variability and enviroclimatic drivers. Results from such evaluations can be used to inform process-level TBM development.

In this paper, we therefore present a framework for (1) diagnosing relationships between NEE and enviroclimatic drivers using atmospheric observations for North America, (2) evaluating the same relationships from NEE simulations from four TBMs participating in the North American Carbon Program (NACP) Regional Interim Synthesis (RIS) [*Huntzinger et al*., 2012], and (3) relating TBM performance to the ability of the TBM to represent relationships between NEE and enviroclimatic drivers that are observable from atmospheric measurements.

2. Data and Methods

2.1. Atmospheric CO_2 Observations

We use continuous atmospheric CO_2 mixing ratio measurements from 35 towers (Figure S1 and Table S1 in the supporting information) available in 2008. The tower network includes the following: (1) nine towers operated by the Global Monitoring Division of NOAA's Earth Research Laboratory [*Andrews et al*., 2014], located in Park Falls, Wisconsin (LEF), Moody, Texas (WKT), West Branch, Iowa (WBI), Boulder Atmospheric Observatory, Colorado (BAO), Argyle, Maine (AMT), South Carolina Tower, South Carolina (SCT) and Walnut Grove, California (WGC), Shenandoah National Park, Virginia (SNP), and Barrow, Alaska (BRW) [*Thoning et al*., 2014]; (2) seven towers supported by the Mid-Continental Intensive project, located in Canaan Valley, West Virginia (CVA), Missouri Ozarks, Missouri (OZA) [*Stephens et al*., 2011], Kewanee, Illinois (KEW), Centerville, Iowa (CEN), Mead, Nebraska (MEA), Round Lake, Missouri (ROL), and Galesville, Wisconsin (GAL) [*Richardson et al*., 2011]; (3) three towers within the Regional Atmospheric Continuous CO_2 Network in the Rocky Mountains (RACCOON) [*Stephens et al*., 2011], located in Storm Peak Lab, Colorado (SPL), Niwot Ridge, Colorado (NWR), and Hidden Peak Snowbird, Utah (HDP); (4) seven towers supported by Environment Canada, located in Fraserdale, Ontario (FRD), Egbert, Ontario (EGB), Candle Lake,

Saskatcheway (CDL), East Trout Lake, Saskatchewan (ETL), Sable Island, Nova Scotia (SBL), Lac LaBiche, Alberta (LLB), and Chibougamau, Quebec (CHI); (5) five Oregon towers operated by Oregon State University [*Göckede et al*., 2010], including the Fir (FIR), Metolius (MET), Yaquina Head (YAH), Mary's Peak (MAP), and Burns Old (NGB); and (6) four additional towers, located at the Harvard Forest, Massachusetts (HFM) [*Urbanski et al*., 2007], Morgan Monroe State Forest, Illinois (MMS) [*Dragoni et al*., 2007; *Schmid et al*., 2000], Southern Great Plains, Oklahoma (SGP), and La Jolla, CA (LJA) [*Keeling et al*., 2005].

CO_2 measurements from these towers were first filtered to exclude data with low-quality flags and extreme outliers (defined as observations that were more than three times the interquartile range away from the upper/lower quantile). The filtered measurements were then averaged to a 3-hourly timescale. The 3-hourly observations were further filtered if they are more than 30 ppm over background air or if their sensitivity to ocean fluxes was greater than 85% of their total sensitivity to ocean and land [*Gourdji et al*., 2012].

For this study, we further avoided measurements that are likely to be strongly affected by errors in atmospheric transport models, as in *Gourdji et al*. [2012] and *Shiga et al*. [2014]: for all tall towers with a height over 300 m, data from all hours of the day are used; only afternoon data are used for most short towers (lower than 100 m), while nighttime data are used for sites in complex terrain (e.g., NWR) (see Table S1 for details). In addition, following *Fang et al*. [2014], we remove data that are strongly influenced by fluxes in only a few grid cells, in order to exclude data that are likely sensitive to any systematic transport model errors [*Göckede et al*., 2010; *Gourdji et al*., 2012; *Peters et al*., 2007]. The effects of boundary conditions [*GLOBALVIEW-CO_2*, 2010] and fossil fuel CO_2 emissions are presubtracted from atmospheric measurements as described in *Fang et al*. [2014].

2.2. Sensitivity of Atmospheric CO_2 Measurements to Surface Fluxes and Simulated Terrestrial Fluxes

The sensitivity of available atmospheric CO_2 measurements to underlying CO_2 fluxes (i.e., footprints, in units of ppmv/(μmol m^{-2} s^{-1})) is derived as in *Gourdji et al*. [2012], using the Stochastic Time-Inverted Lagrangian Transport (STILT) model [*Lin et al*., 2003] driven by the Weather Research and Forecast (WRF) model [*Skamarock and Klemp*, 2008].

Simulated NEE at a 3-hourly and 1°×1° resolution is obtained from the NACP RIS runs [*Huntzinger et al*., 2012] of four TBMs: CASA-GFED [*van der Werf et al*., 2006], SiB3 [*Baker et al*., 2008], ORCHIDEE [*Krinner et al*., 2005], and VEGAS2 [*Zeng et al*., 2005]. These four simulations were selected for analysis because of the availability of 3-hourly NEE flux output. Details of those models are shown in *Fang et al*. [2014] and *Huntzinger et al*. [2012].

2.3. Enviroclimatic Drivers

In addition to the data sets above, this study also uses multiple enviroclimatic driver data sets (all at a 3-hourly and 1°×1° resolution) from the North American Regional Reanalysis (NARR) [*Mesinger et al*., 2006]. These drivers include precipitation, as well as two derived precipitation indices, namely the average precipitation over the previous 16 and 30 day intervals. These latter two are used to capture the potential lagged responses of NEE to precipitation. We also include specific humidity, relative humidity, and air temperature (at 2 m above ground), as well as downward shortwave radiation, snow depth, and snow cover. This superset of NARR variables primarily relates to water fluxes and availability, temperature and shortwave radiation. Note that the enviroclimatic driver data sets used here (from NARR) do not necessarily correspond to the data used to drive the TBMs assessed in this study: SiB3 uses NARR data sets, while the other models use data from other sources.

2.4. Statistical Framework Linking CO_2 Observations to Enviroclimatic Drivers

The main goal of this study is to evaluate TBM performance in simulating the relationship between fine-scale (defined at 1°×1° spatial and 3-hourly temporal resolution) NEE spatiotemporal variability and major enviroclimatic drivers within specific biomes and months. This goal is achieved through an atmospheric inversion framework designed to identify the enviroclimatic drivers that best represent the fine-scale spatiotemporal variability of NEE within 84 biome-month combinations (i.e., seven aggregate North American biomes defined as in Figure S1 and 12 months of the year 2008). Due to the coverage of the observation network, results are only interpreted for the four biomes identified to be better constrained by *Fang et al*. [2014], namely, (1) boreal forests and taiga; (2) temperate coniferous forests; (3) temperate grasslands, savannas, and shrublands; and (4) temperate broadleaf and mixed forests (Figure S1), where atmospheric CO_2 measurements provide sufficient constraints to inform the underlying spatiotemporal

patterns of NEE. The framework is applied both to real atmospheric CO_2 observations and to simulated observations based on NEE as predicted by each of the examined TBMs.

Similarly to *Fang et al*. [2014], we model the atmospheric observations using a linear mixed model, building on the geostatistical inverse modeling framework [*Gourdji et al*., 2010, 2012; *Michalak et al*., 2004], to relate enviroclimatic drivers to NEE fluxes that are not directly observed but that can be assessed via their influence on atmospheric CO_2 measurements:

$$\mathbf{z} = \mathbf{H}\mathbf{X}\boldsymbol{\beta} + \mathbf{H}\boldsymbol{\xi} + \boldsymbol{\varepsilon} \tag{1}$$

Where $\mathbf{z}$ is an $n \times 1$ vector of atmospheric CO_2 observation (with the influence of boundary conditions and fossil fuel emissions removed see section 2.1). $\mathbf{H}$ ($n \times m$) are the sensitivity footprints as quantified using STILT (see section 2.2), representing the sensitivity of each observation (dimension of n) to flux at 3-hourly and $1° \times 1°$ resolution (dimension of m); $\mathbf{X}$ ($m \times p$) is a matrix of p ancillary variables used to explain the NEE spatiotemporal variability; $\boldsymbol{\beta}$ is a $p \times 1$ vector that represents the unknown drift coefficients describing the relationships between ancillary variables (i.e., columns of $\mathbf{X}$) and NEE; and $\mathbf{X}\boldsymbol{\beta}$ together thus represents a statistical model of the trend for describing NEE. Each ancillary variable can be either simulated NEE from a TBM in a specific biome-month as in *Fang et al*. [2014] or a NARR variable, both defined only within a specific biome-month combination, i.e., defined only for those rows corresponding to fluxes within a specific biome-month combination, while the remainder of the column is filled with zeros. $\boldsymbol{\xi}$ ($m \times 1$) represents the portion of the variability of NEE that is evident from the atmospheric observations but that cannot be explained by the ancillary variables in $\mathbf{X}$. Finally, $\boldsymbol{\varepsilon}$ ($n \times 1$) is the model-data mismatch term that represents any discrepancies between observed ($\mathbf{z}$) and modeled ($\mathbf{H}\mathbf{X}\boldsymbol{\beta} + \mathbf{H}\boldsymbol{\xi}$) CO_2 mixing ratios. Except as detailed above, all variables in equation (1) are as defined as in *Fang et al*. [2014].

The selection of ancillary variables to be included in $\mathbf{X}$ represents a classical statistical model selection problem, i.e., determining which predictor variables (ancillary variables as columns in $\mathbf{X}$, either NARR enviroclimatic drivers or simulated NEE) are important in explaining the variability in the atmospheric CO_2 measurements. As in *Fang et al*. [2014], we use the Bayesian information criterion (BIC) to select the optimal set of covariates, where BIC takes into account both the goodness of fit and the numbers of ancillary variables in each candidate model to inform model selection.

Finally, the estimated drift coefficients $\hat{\boldsymbol{\beta}}$ associated with each selected ancillary variable and their uncertainty covariances $\left(\mathbf{V}\hat{\boldsymbol{\beta}}\right)$ are obtained as in *Gourdji et al*. [2012]:

$$\hat{\boldsymbol{\beta}} = \left((\mathbf{H}\mathbf{X}_c)^T \boldsymbol{\Sigma}^{-1} (\mathbf{H}\mathbf{X}_c)\right)^{-1} (\mathbf{H}\mathbf{X}_c)^T \boldsymbol{\Sigma}^{-1} \mathbf{z} \tag{2}$$

$$\mathbf{V}\hat{\boldsymbol{\beta}} = \left(\mathbf{X}_c{}^T \mathbf{H}^T \boldsymbol{\Sigma}^{-1} \mathbf{H}\mathbf{X}_c\right)^{-1} \tag{3}$$

Here T is the matrix transpose operator, $\mathbf{X}_c$ includes the final selected ancillary variables, the $\hat{\boldsymbol{\beta}}$ values are the estimated drift coefficients (i.e., fixed effects) in the linear model, and $\boldsymbol{\Sigma}$ is the covariance of the model residuals (i.e., the covariance of $\mathbf{H}\boldsymbol{\xi} + \boldsymbol{\varepsilon}$), defined as follows:

$$\boldsymbol{\Sigma} = \mathbf{H}\mathbf{Q}\mathbf{H}^T + \mathbf{R} \tag{4}$$

where $\mathbf{Q}$ ($m \times m$) is a covariance matrix describing how $\boldsymbol{\xi}$ is correlated in space and time and is modeled using an exponential covariance model, while $\mathbf{R}$ ($n \times n$) is a diagonal covariance matrix with the variance of $\boldsymbol{\varepsilon}$. The specific parameters defining $\mathbf{Q}$ and $\mathbf{R}$ vary between the various experiments and are described in section 2.5. The diagonal elements of $\mathbf{V}_{\hat{\boldsymbol{\beta}}}$ represent the uncertainties of the estimated $\hat{\boldsymbol{\beta}}$ values.

This framework is built on linear relationships between the NEE spatiotemporal variability and enviroclimatic drivers. Such relationships are chosen because, although more complex relationships certainly exist at the process level, earlier studies have found that even simple linear relationships can explain a large portion of the variability in carbon fluxes from site level to hemispheric and global scales, and from daily to annual scales [*Mueller et al*., 2010; *Piao et al*., 2013; *Schneising et al*., 2014; *Wang et al*., 2013; *Yadav et al*., 2010]. Such relationships also facilitate the intercomparison of the derived relationships across drivers and across models, and yield a parsimonious model that can effectively leverage the limited information content of atmospheric observations.

2.5. Experiments

In this section, we describe the experiments conducted to fulfill the objectives outlined in section 1.

The RD-NARR experiment uses real atmospheric CO_2 data (RD) and NARR data as ancillary variables (NARR) and is designed (1) to identify the enviroclimatic drivers within specific biome-month combinations that contribute most to explaining the observed variability in atmospheric CO_2 and (2) to estimate the drift coefficients defining the linear relationships between those drivers and the spatiotemporal variability of NEE within those biome-month combinations. The covariance parameters needed for **Q** and **R** are estimated using the Restricted Maximum Likelihood approach using the atmospheric observations themselves and the final selected ancillary variables ($\mathbf{X}_c$) [e.g., *Gourdji et al*., 2010, 2012; *Michalak et al*., 2004].

The SD-NARR suite of experiments uses synthetic atmospheric CO_2 data (SD) generated using simulated NEE from each of the four examined TBMs and the footprints in **H** (i.e., $\mathbf{z}_{SD} = \mathbf{HS}_{TBM}$), and NARR data as ancillary variables (NARR). These four experiments are designed to identify the enviroclimatic drivers within specific biome-month combinations that would contribute most to explaining the observed variability in atmospheric CO_2 if indeed the true fluxes were consistent with those simulated by one of the TBMs examined here. In analogy to the RD-NARR experiment, these experiments also estimate the drift coefficients defining the linear relationship between those drivers and the spatiotemporal variability of NEE within those biome-month combinations. For simplicity, the synthetic observations do not include the influence of fossil fuel emissions or boundary conditions. To ensure a fair comparison with the RD-NARR experiment, however, in each case the synthetic observations include model-data mismatch errors with variances equal to those estimated from RD-NARR and included in **R**. Those model-data mismatch errors represent the transport model, measurements and aggregation errors, as well as errors in the boundary conditions. To be conservative, the **Q** parameters for each SD-NARR experiment are estimated based on the full variability of NEE from a particular TBM [*Gourdji et al*., 2008, 2010; *Mueller et al*., 2008].

We use results obtained from the RD-one-$\xi\varepsilon$ suite of experiments in *Fang et al*. [2014] to complete the analysis, which used real atmospheric CO_2 data (RD) and fluxes from one of the individual TBMs as the ancillary variables for each of the four experiments. This experiment was designed to identify whether the spatiotemporal variability of NEE as simulated by a specific TBM contributed substantially toward explaining the observed variability in atmospheric CO_2.

Results for all experiments are interpreted for the four biomes considered here (boreal forests and taiga; temperate coniferous forests; temperate grasslands, savannas, and shrublands; and temperate broadleaf and mixed forests), as identified in *Fang et al*. [2014]. Together, these experiments make it possible to explore the skill of TBMs in simulating the relationship between NEE spatiotemporal variability and major enviroclimatic drivers.

3. Results

3.1. Relationships Between NEE Spatiotemporal Variability and Enviroclimatic Drivers as Observed From Atmospheric Measurements

Results from the case study linking atmospheric CO_2 observations to enviroclimatic drivers (RD-NARR) show that relationships between NEE spatiotemporal variability and enviroclimatic drivers can indeed be inferred from atmospheric CO_2 data. Overall, linear relationships are identified for 75% of biome-month combinations for the four biomes previously shown to be relatively well constrained by atmospheric CO_2 observations (Figure 1). Such linear relationships have also previously been observed in site level flux studies [*Hui et al*., 2003; *Law et al*., 2002; *Mueller et al*., 2010; *Vargas et al*., 2010; *Yadav et al*., 2010; *Yu et al*., 2013]. One exception is during summer over temperate coniferous forests, where none of the enviroclimatic drivers are identified. As atmospheric data have been shown to be sensitive to the NEE variability within this biome [*Fang et al*., 2014], the failure to identify enviroclimatic relationships may indicate that simple linear relationships do not capture a substantial portion of the actual variability for this biome.

Relationships between NEE spatiotemporal variability and enviroclimatic drivers are identified both (1) for biome-month combinations where TBMs were previously shown by *Fang et al*. [2014] to have relatively high skill in representing the spatiotemporal variability of NEE, e.g., the growing season (May–September, Figure 1), and (2) even for biome-month combinations where TBMs performed less reliably, e.g., the

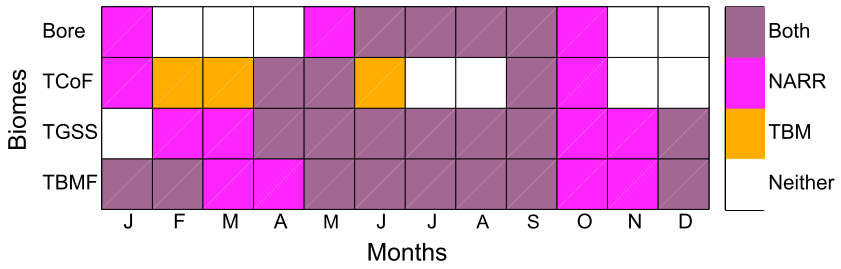

Figure 1. The biome (rows)-month (columns) combinations within which, neither enviroclimatic drivers nor TBMs (white), only enviroclimatic drivers (magenta), only TBMs (orange), or both enviroclimatic drivers and TBMs (dark purple) are identified as important for explaining the NEE variability using actual atmospheric CO_2 measurements. Only results from four better constrained biomes are shown, namely: "Bore": boreal forests and taiga; "TCoF": temperate coniferous forests; "TGSS": temperate grasslands, savannas, shrublands; and "TBMF": temperate broadleaf and mixed forests.

transition seasons (March–April and October–November, Figure 1). In other words, a linear combination with enviroclimatic drivers can explain a portion of NEE variability for more biome-months than can process-based models. This is a rather surprising outcome, as it means that linear relationships with enviroclimatic drivers have stronger explanatory power than do TBMs in representing flux variability in some biomes and months. This finding implies that TBMs may not capture the relationships between flux variability and enviroclimatic drivers evident from atmospheric observations. Exploring which enviroclimatic drivers are related to flux patterns within biome-months where TBMs perform better, and where they perform less well, could therefore provide insights about how well specific processes are represented within TBMs. For example, *Fang et al*. [2014] suggested that the seasonal variability in TBM performance may be attributable to changes in the dominant enviroclimatic drivers across seasons at the scales observable through atmospheric measurements. The experiments conducted here make it possible to test this hypothesis.

The approach applied here makes it possible, for the first time, to characterize the relationships between enviroclimatic drivers and the spatiotemporal variability of fluxes within specific biome-month combinations directly from atmospheric CO_2 observations, and to do so at scales similar to typical resolutions of TBMs run for regional to continental analyses. Figure 2 shows the drift coefficients $(\hat{\boldsymbol{\beta}})$ between enviroclimatic drivers and the spatiotemporal variability of NEE for each month, and within each of the four better constrained biomes examined here. Snow depth and snow cover are not included in the figure because they were only found to be good predictors for a total of three biome-month combinations. The presented drift coefficients are based on enviroclimatic driver variables that have all been normalized ($\mu = 0$; $\sigma = 1$), such that their relative magnitudes are representative of each driver's relative impact on flux patterns.

Results in Figure 2 indicate that shortwave radiation plays a dominant role in determining NEE spatiotemporal variability in all four biomes during the growing season, which is also the time when TBMs perform best in explaining flux patterns. During other months (e.g., the transition seasons), on the other hand, shortwave radiation no longer acts as a dominant driver; instead, its relationship with NEE variability is only apparent for some biome-months, and the magnitude of its drift coefficient is comparable to that of other drivers such as specific humidity, precipitation, and/or temperature. Regardless of season, shortwave radiation is always associated with a negative drift coefficient, indicating that an increase in shortwave radiation is associated with increased carbon uptake. This result is consistent with the known relationship between radiation and photosynthesis and with earlier site-level studies [*Mueller et al*., 2010; *Yadav et al*., 2010].

The inferred relationships between NEE and other drivers differ from that with shortwave radiation. A relationship with specific humidity is apparent during spring and fall and is associated with a positive drift coefficient, indicating a decrease in carbon uptake (or increase in carbon release) associated with increased specific humidity. This relationship likely reflects the fact that heterotrophic respiration increases with temperature and water abundance in most regions [*Ise and Moorcroft*, 2006; *Lloyd and Taylor*, 1994]. A relationship with precipitation is identified mainly during winter and summer months, and an increase in precipitation is typically associated with reduced carbon uptake (or increased carbon release). This is consistent with pulses of respiration following rain events [*Baldocchi*, 2008; *Huxman et al*., 2004] and the relationships between carbon fluxes and precipitation on short temporal scale (i.e., daily to weekly) inferred by earlier studies based on eddy covariance measurement [*Mueller et al*., 2010; *Yadav et al*., 2010].

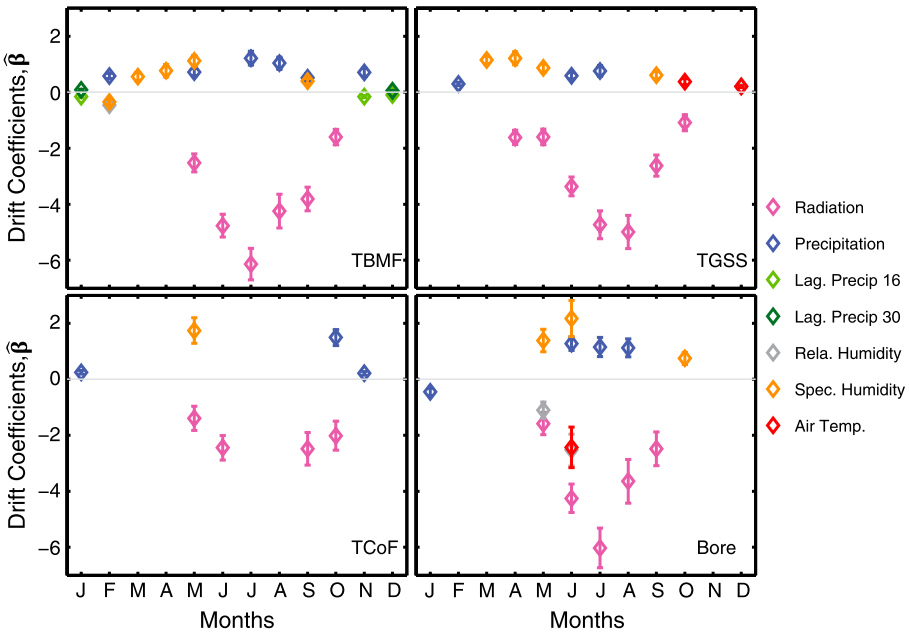

Figure 2. The estimated drift coefficients $(\hat{\boldsymbol{\beta}})$ associated with enviroclimatic drivers identified as important in explaining the NEE spatiotemporal variability using actual atmospheric CO_2 measurements over temperate broadleaf and mixed forests (TBMF); temperate grasslands, savannas, and shrublands (TGSS); temperate coniferous forests (TCoF), and boreal forests and taiga (Bore). The drivers include shortwave radiation (purple), precipitation (blue), 16 day lagged precipitation (Lag. Precip 16, green), 30 day lagged precipitation (Lag. Precip 30, dark green), relative humidity (Rela. Humidity, gray), specific humidity (Spec. Humidity, orange), and air temperature (Air Temp., red). Error bars show the uncertainty range of $\hat{\boldsymbol{\beta}}$, i.e., $\pm\sigma\hat{\boldsymbol{\beta}}$, the square root of the diagnoal elements of the uncertainty covariances $(\mathbf{V}\hat{\boldsymbol{\beta}})$.

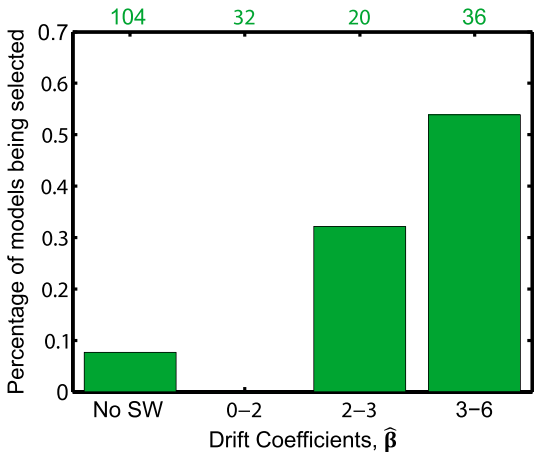

Figure 3. The likelihood of a TBM being selected as important in explaining the NEE spatiotemporal variability using actual atmospheric measurements across all examined biome-month combinations and TBMs, binned as follows: No SW (shortwave radiation is not identified as an important covariate), "0–2" (the impact of shortwave radiation is relatively weak $(0 \le \hat{\boldsymbol{\beta}} < 2)$); "2–3" (the impact of shortwave radiation is moderate $(2 \le \hat{\boldsymbol{\beta}} < 3)$) "3–6" (the impact of shortwave radiation is strong $(\hat{\boldsymbol{\beta}} \ge 3)$). Green values on the top of the plot indicate the number of biome-month-TBM combinations in each category.

3.2. Relationships Between NEE Spatiotemporal Variability and Enviroclimatic Drivers as Implied by TBMs

The findings in the previous subsection suggest a connection between key enviroclimatic drivers and model performance, with periods when TBMs perform well corresponding to periods when NEE spatiotemporal patterns are strongly related to incoming shortwave radiation (i.e., during the growing season). Model performance is weaker, on the other hand, during transition seasons when other variables (e.g., specific humidity and precipitation) are more directly related to NEE. This connection is further illustrated in Figure 3, which shows the overall likelihood of a model being identified as representing a substantial portion of the NEE spatiotemporal variability (across all 4 models, all 4 biomes, and all 12 months), as a function of the magnitude of the estimated drift coefficient $(\hat{\boldsymbol{\beta}})$ associated with shortwave radiation. When shortwave radiation is not identified as an important covariate ("No SW"), or when its impact on NEE spatiotemporal variability is weak $(0 \le \hat{\boldsymbol{\beta}} < 2)$ TBMs are almost never identified as representing flux patterns consistently with what

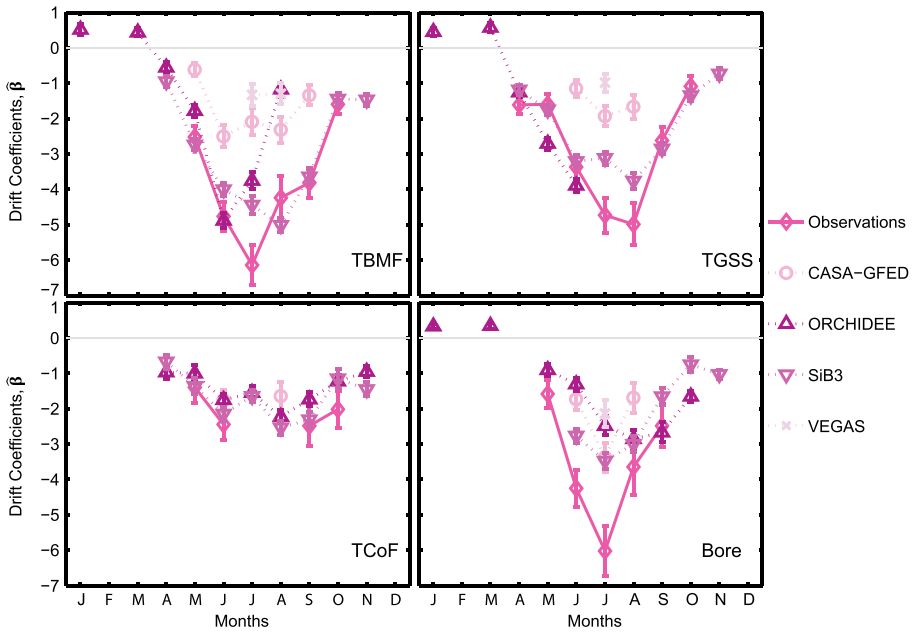

Figure 4. The estimated drift coefficients $(\hat{\boldsymbol{\beta}})$ associated with shortwave radiation for cases where it is identified as important in explaining the NEE spatiotemporal variability using actual atmospheric CO_2 measurements (solid line, diamonds) and using synthetic observations assuming underlying fluxes as simulated by each of the four TBMs (dotted lines), with CASA-GFED represented as circles, ORCHIDEE as upward pointing triangles, SiB3 as downward pointing triangles, and VEGAS as crosses, over temperate and broadleaf mixed forests (TBMF); temperate grasslands, savannas and shrublands (TGSS); temperate coniferous forests (TCoF); and boreal forests and taiga (Bore). Error bars show the uncertainty range of $\hat{\boldsymbol{\beta}}$, i.e., $\pm\sigma\hat{\boldsymbol{\beta}}$, the square root of the diagnoal elements of the uncertainty covariances $(\mathbf{V}\hat{\boldsymbol{\beta}})$.

can be observed from atmospheric measurements. TBMs perform better when the influence of shortwave is stronger $(2 \le \hat{\boldsymbol{\beta}} < 3)$, and they are found to represent a substantial portion of the observed CO_2 variability more than 50% of the time when shortwave radiation dominates $(\hat{\boldsymbol{\beta}} \ge 3)$. Although the specific cutoffs for these ranges are somewhat subjective, the clear conclusion is that TBMs represent the spatiotemporal patterns of NEE within specific biomes and months better when shortwave radiation is a controlling factor for NEE patterns.

Taken together, these results indicate that TBMs represent the impact of radiation on NEE better than the impact of other enviroclimatic drivers, such as temperature and precipitation. This conclusion is further confirmed when performing a similar analysis, but using synthetic atmospheric observations generated using each of the examined TBMs (Figures S2–S5).

The relationships between shortwave radiation and NEE spatiotemporal variability inferred from synthetic observations using TBM-generated fluxes are relatively consistent with those inferred using real observations (Figure 4). TBMs generally capture the sign as well as the seasonal variation of the relationship between NEE and shortwave radiation evident from atmospheric measurements.

However, they typically underestimate the peak of the $\hat{\boldsymbol{\beta}}$ value, and hence the response of NEE to shortwave radiation, especially for temperate and boreal forests. This result is consistent with the biased-low carbon uptake and light use efficiency (LUE) found in site level studies during summers [*Richardson et al*., 2012; *Schaefer et al*., 2012]. Those summer biases have been attributed to model underestimate of the peak leaf area index (LAI) and therefore photosynthesis [*Richardson et al*., 2012]. LUE is related to various parameters, such as potential conversion efficiency or carbon yield of absorbed energy and the stress terms related to environmental factors [*J. Wang et al*., 2014; *Ågren and Andersson*, 2012; *Cao et al*., 2004] . It is possible that during summers, either the conversion efficiency is underestimated and/or the stress terms are overestimated. This bias is particularly strong over boreal forests and taiga, where the observations imply a similar relationship to radiation as for temperate broadleaf and mixed forests, while the models suggest a substantially weaker relationship. This result is consistent with *Barr et al*. [2007], who suggested that the productivity of boreal forests may be similar to that of temperate forests.

Additionally, during the transition seasons, TBMs do not capture the timing of the emergence and disappearance of shortwave radiation as an important factor. For example, for temperate broadleaf and mixed forest, shortwave radiation is first identified as an important driver from synthetic observations generated using NEE from ORCHIDEE and SiB3, one month earlier than it is when using real observations (Figures S3 and S4). This finding is consistent with earlier work that also pointed to challenges of TBMs in simulating phenology and hence the seasonality of biospheric CO_2 flux [*Richardson et al*., 2012; *Schaefer et al*., 2012; *Schwalm et al*., 2010].

Relative to shortwave radiation, TBMs have more limited skill in representing the relationships associated with temperature and water availability (Figures S2–S5 versus Figure 2). First, for about 80% of cases, those enviroclimatic drivers (e.g., temperature, specific humidity, and precipitation) are associated with negative drift coefficients (i.e., increase in sink or decrease in source), while they are associated with positive drift coefficients (i.e., decrease in sink or increase in source) based on the real observations in about 90% of cases. One example of this contrast is the impact of summertime precipitation. Second, relative to relationships inferred from real observations, relationships between enviroclimatic drivers and NEE patterns are evident for fewer biome-months when using synthetic observations based on TBM-generated NEE, and these relationships occur during different months. For example, relative humidity is generally selected as an important driver during spring and fall from real observations, but it is mostly identified as a key explanatory variable during the summer based on TBMs. In some cases, both the timing and the sign of the relationship are inconsistent, such as in the case of specific humidity over temperate grassland, savannas, and shrublands, as well as over boreal forests and taiga.

Although our results are based on using NARR variables as the enviroclimatic drivers, we find that the choice of the NARR data source and whether these same data were also used as driver data by the examined TBMs are unlikely to significantly affect results. For example, SiB3 is driven by the same set of NARR drivers, and yet the relationships between SiB3 NEE and NARR enviroclimatic drivers are not noticeably stronger relative to the remaining models, which use other driver data sets (Figures S2–S5). Furthermore, ORCHIDEE (Figure S3) and VEGAS2 (Figure S5) both use the same set of drivers [*Huntzinger et al*., 2012], and yet we observe substantial differences in the relationships between their NEE and NARR data. These examples support the idea that the choice of drivers is not the predominant determinant of the results observed here. Instead, the differences in the simulated relationships between NEE and enviroclimatic drivers are likely more strongly attributable to model internal structure, although this hypothesis could be further tested by repeating the experiments outlined here using a set of models driven by a consistent set of driver data.

3.3. Implications for Continued TBM Development

The results of the analysis presented here point to three possible areas of opportunity for further TBM development.

The first is to exploit data sets that can help to inform the covariation between the seasonality of phenology and the seasonality of the dominance of radiation as a strong explanatory factor for NEE. Recent intercomparisons have pointed to biases in TBMs in both the seasonality of gross primary product ion (GPP) and the magnitude of its summertime peak [*Schaefer et al*., 2012; *Richardson et al*., 2012; *Schwalm et al*., 2010; *Abramowitz et al*., 2008], while results presented here show a similar picture for the role of radiation in explaining the spatiotemporal variability of NEE within specific biomes and months. The increasing availability of global data sets that capture the seasonality of phenology and fluxes may provide a path toward resolving these discrepancies. For example, the incorporation of satellite-based global measurements of solar-induced fluorescence (SIF) [*Frankenberg et al*., 2013; *Guanter et al*., 2014] into dynamic vegetation models has been shown to lead to improvements in the structure of the seasonal cycle of GPP [*Joiner et al*., 2011; *Parazoo et al*., 2014]. In addition, SIF can also constrain moisture impacts on stomatal conductance and GPP [*Joiner et al*., 2011; *Lee et al*., 2013; *Parazoo et al*., 2014], thus providing insights into seasonal water stress.

The second area is to further explore how the relationship between fluxes and enviroclimatic drivers varies under different environmental conditions (e.g., temperature and humidity). Such analyses, even if conducted at finer spatial scales such as those represented by eddy covariance observations, could help to identify conditions under which the relationship of fluxes with temperature and humidity as represented in TBMs differ from observations. These insights could help to explain why TBMs appear not to capture the timing of the emergence of temperature and humidity as key drivers, or the sign of their relationships to NEE

at the scales examined here. To do so, the response of both observed and model-simulated GPP, respiration, and NEE to temperature and humidity would need to be examined at intraseasonal timescales (e.g., hourly and daily) within different humidity and temperature regimes. This strategy is supported by the fact that earlier studies have shown that the response of GPP to temperature and humidity varies strongly across different environmental conditions [e.g., *Schaefer et al*., 2012]. Using humidity as an example, *Schaefer et al*. [2012] showed that the observed sensitivity of GPP to humidity is different when relative humidity is less than 40%, between 40 and 70% and above 80%. The responses of heterotrophic and autotrophic respiration to humidity and temperature have also been shown to vary under different environmental conditions [*Bronson et al*., 2008; *Gaumont-Guay et al*., 2009; *Lloyd and Taylor*, 1994; *Matthias et al*., 2014].

The final area focuses on the scale dependence of the relationship between flux and precipitation. Results presented here suggest that model-simulated NEE is negatively correlated to precipitation while CO_2 observations suggest the opposite at the 3-hourly temporal scale. Eddy covariance measurements of GPP, respiration and NEE could be used to examine how the relationships between fluxes and precipitation varies across temporal scales, and how this scale dependency is represented in TBMs. Past work has shown that this relationship is indeed scale dependent, with precipitation leading to short-term pulses in respiration [*Baldocchi*, 2008; *Gourdji et al*., 2012; *Huxman et al*., 2004; *Mueller et al*., 2010; *Yadav et al*., 2010]. The response of NEE here is consistent with this earlier work. However, we find that all four examined TBMs consistently show the opposite relationship, more consistent with the expected relationship at longer timescales, where increased precipitation leads to increased carbon uptake [*Chimner and Welker*, 2011; *Piao et al*., 2013; *Rigge et al*., 2013].

4. Conclusions

In this paper, we apply an atmospheric-inversion-based framework to investigate the responses of net ecosystem CO_2 exchange (NEE) to enviroclimatic drivers at the 3-hourly and $1° \times 1°$ resolution within North American biomes in 2008. We further evaluate the capability of a subset of TBMs participating in the North American Carbon Program (NACP) Regional Interim Synthesis (RIS) in representing those responses within specific biome-month combinations.

We find that the relationships between NEE spatiotemporal variability and enviroclimatic drivers can be inferred from atmospheric CO_2 measurements for 75% of the biome-month combinations over four better constrained biomes (i.e., boreal forests and taiga; temperate coniferous forests; temperate grasslands, savannas, and shrublands; and temperate broadleaf and mixed forests).

For the first time, we are able to characterize, directly from atmospheric CO_2 observations, the relationships between enviroclimatic drivers and the spatiotemporal variability of NEE within a majority of North American biomes. Results indicate a strong seasonality in relationships between NEE and drivers. Shortwave radiation is clearly the dominant driver affecting NEE patterns over all four biomes during the growing season, with its influence being highest in summer; during the nongrowing season, however, its role becomes either comparable to that of other drivers or not apparent in our framework. Specific humidity is found to be a more important driver mainly during spring and fall. Precipitation (and related drivers) is important during both winter and summer, although its influence in summer is weaker than that of shortwave radiation.

By comparing the inferred relationships between NEE patterns and enviroclimatic drivers to the performance of TBMs in simulating NEE patterns, a connection between key enviroclimatic drivers and model performance emerges. TBMs typically perform well when NEE spatiotemporal patterns are strongly related to incoming shortwave radiation (i.e., during the growing season), while their performance is weaker during transition seasons when other drivers (e.g., specific humidity) are more strongly related to NEE.

Such a connection suggests that TBMs may have stronger skill in representing the impact of shortwave radiation on NEE than that of the drivers related to temperature and water availability. TBMs are further found to capture both the sign and the seasonal variation of the relationships between NEE and shortwave radiation. In contrast, their skill in representing the relationships associated with temperature and water availability is more limited, both in representing the sign and timing of the relationships.

The work presented here complements earlier studies on TBM model evaluation by using an empirical statistical approach to assess NEE patterns at 3-hourly and $1° \times 1°$ resolution, a typical resolution of TBMs run for regional to continental analyses. It also complements previous assessments that focused on aggregated or plot scales in that

it focuses more directly on the mechanistic representation of processes within the TBMs. By doing so, this study sheds new light on possible avenues for further TBM development. Those areas include the following: (1) how and when shortwave radiation emerges and disappears as a key driver controlling NEE patterns; (2) the responses of NEE to temperature and humidity at intraseasonal scales (e.g., hourly, daily, and monthly); (3) the scale dependency of the precipitation impact on NEE.

Acknowledgments

This work is funded by the National Aeronautics and Space Administration (NASA) under grants NNX12AB90G and NNX12AM97G. The authors thank the biospheric modelers participating in the NACP Regional Interim Synthesis, specifically, Ning Zeng, Ian Baker, Nicolas Viovy, and James Randerson for providing the model results used in the analysis. We thank Deborah Huntzinger for downscaling the CASA-GFED and VEGAS2 fluxes to 3-hourly temporal resolution. Atmospheric and Environmental Research Inc. (AER) and, in particular, Thomas Nehrkorn, John Henderson, and Janusz Eluszkiewicz performed the WRF-STILT simulations and provided the sensitivity footprints. We gratefully acknowledge the efforts of the PIs of the various towers providing continuous atmospheric CO_2 observations, which were instrumental both for this and several earlier analyses. The sites BRW, WGC, SNP, SCT, AMT, WBI, BAO, LEF, and WKT are part of NOAA's Global Greenhouse Gas Reference Network operated by the Global Monitoring Division of NOAA's Earth System Research Laboratory with additional support from NOAA's Climate Program Office and are a contribution to the North American Carbon Program. The installation of CO_2 sampling equipment was made possible at AMT, by a grant from the National Science Foundation Biocomplexity in the Environment Program (ATM-0221850), at SNP, by the University of Virginia, and at SCT by funding provided by the DOE Office of Science–Terrestrial Carbon Processes program and performed under contract DE-AC09-08SR22470. Savannah River National Laboratory (SNRL) is operated by Savannah River Nuclear Solutions, LLC under contract DE-AC09-08SR22470 with the U.S. Department of Energy. WGC measurements were supported by a combination of the California Energy Commission's Public Interest Environmental Research Program to the Lawrence Berkeley National Laboratory under contract DE-AC02-05CH11231 and NOAA. Research at CVA, OZA, KEW, CEN, MEA, ROL, and GAL was sponsored by the U.S. Department of Energy Office of Science TCP program (DE-FG02-06ER64315) and by the U.S. Department of Commerce, NOAA office of Global Programs (NA08OAR4310533). The five Oregon sites FIR, MET, YAH, MAP, NGB were supported by NOAA (NA11OAR4310056). The research at the MMS site was sponsored by the U.S.

References

Abramowitz, G., R. Leuning, M. Clark, and A. Pitman (2008), Evaluating the performance of land surface models, *J. Clim.*, *21*(21), 5468–5481, doi:10.1175/2008JCLI2378.1.

Ågren, G. I., and F. O. Andersson (2012), *Terrestrial Ecosystem Ecology: Principles and Applications*, 345 pp., Cambridge Univ. Press, New York.

Andrews, A. E., et al. (2014), CO_2, CO, and CH_4 measurements from tall towers in the NOAA Earth System Research Laboratory's Global Greenhouse Gas Reference Network: Instrumentation, uncertainty analysis, and recommendations for future high-accuracy greenhouse gas monitoring efforts, *Atmos. Meas. Tech.*, *7*(2), 647–687, doi:10.5194/amt-7-647-2014.

Baker, I. T., L. Prihodko, A. S. Denning, M. Goulden, S. Miller, and H. R. da Rocha (2008), Seasonal drought stress in the Amazon: Reconciling models and observations, *J. Geophys. Res.*, *113*, G00B01, doi:10.1029/2007JG000644.

Baldocchi, D. (2008), TURNER REVIEW No. 15. "Breathing" of the terrestrial biosphere: Lessons learned from a global network of carbon dioxide flux measurement systems, *Aust. J. Bot.*, *56*(1), 1–26, doi:10.1071/BT07151.

Barr, A. G., T. A. Black, E. H. Hogg, T. J. Griffis, K. Morgenstern, N. Kljun, A. Theede, and Z. Nesic (2007), Climatic controls on the carbon and water balances of a boreal aspen forest, 1994–2003, *Global Change Biol.*, *13*(3), 561–576, doi:10.1111/j.1365-2486.2006.01220.x.

Beer, C., et al. (2010), Terrestrial gross carbon dioxide uptake: Global distribution and covariation with climate, *Science*, *329*(5993), 834–838, doi:10.1126/science.1184984.

Bronson, D. R., S. T. Gower, M. Tanner, S. Linder, and I. Van Herk (2008), Response of soil surface CO_2 flux in a boreal forest to ecosystem warming, *Global Change Biol.*, *14*(4), 856–867, doi:10.1111/j.1365-2486.2007.01508.x.

Cao, M., S. D. Prince, J. Small, and S. J. Goetz (2004), Remotely sensed interannual variations and trends in terrestrial net primary productivity 1981-2000, *Ecosystems*, *7*(3), 233–242, doi:10.1007/s10021-003-0189-x.

Chimner, R., and J. Welker (2011), Influence of grazing and precipitation on ecosystem carbon cycling in a mixed-grass prairie, *Pastoralism*, *1*(1), 1–15, doi:10.1186/2041-7136-1-20.

Cox, P. M., D. Pearson, B. B. Booth, P. Friedlingstein, C. Huntingford, C. D. Jones, and C. M. Luke (2013), Sensitivity of tropical carbon to climate change constrained by carbon dioxide variability, *Nature*, *494*(7437), 341–344, doi:10.1038/nature11882.

Dragoni, D., H. P. Schmid, C. S. B. Grimmond, and H. W. Loescher (2007), Uncertainty of annual net ecosystem productivity estimated using eddy covariance flux measurements, *J. Geophys. Res.*, *112*, D17102, doi:10.1029/2006JD008149.

Fang, Y., A. M. Michalak, Y. P. Shiga, and V. Yadav (2014), Using atmospheric observations to evaluate the spatiotemporal variability of CO_2 fluxes simulated by terrestrial biospheric models, *Biogeosciences*, *11*(23), 6985–6997, doi:10.5194/bg-11-6985-2014.

Frankenberg, C., J. Berry, L. Guanter, and J. Joiner (2013), Remote sensing of terrestrial chlorophyll fluorescence from space, SPIE Newsroom, 19 Feb., doi:10.1117/2.1201302.004725.

Gaumont-Guay, D., T. A. Black, H. McCaughey, A. G. Barr, P. Krishnan, R. S. Jassal, and Z. Nesic (2009), Soil CO_2 efflux in contrasting boreal deciduous and coniferous stands and its contribution to the ecosystem carbon balance, *Global Change Biol.*, *15*(5), 1302–1319, doi:10.1111/j.1365-2486.2008.01830.x.

GLOBALVIEW-CO_2 (2010), *Cooperative Atmospheric Data Integration Project—Carbon Dioxide (2010)* [CD-ROM], NOAA ESRL Global Monitoring Division, Boulder, Colo. [Available at ftp.cmdl.noaa.gov, Path: ccg/co2/GLOBALVIEW].

Göckede, M., D. P. Turner, A. M. Michalak, D. Vickers, and B. E. Law (2010), Sensitivity of a subregional scale atmospheric inverse CO_2 modeling framework to boundary conditions, *J. Geophys. Res.*, *115*, D24112, doi:10.1029/2010JD014443.

Gourdji, S. M., K. L. Mueller, K. Schaefer, and A. M. Michalak (2008), Global monthly averaged CO_2 fluxes recovered using a geostatistical inverse modeling approach: 2. Results including auxiliary environmental data, *J. Geophys. Res.*, *113*, D21115, doi:10.1029/2007JD009733.

Gourdji, S. M., A. I. Hirsch, K. L. Mueller, V. Yadav, A. E. Andrews, and A. M. Michalak (2010), Regional-scale geostatistical inverse modeling of North American CO_2 fluxes: A synthetic data study, *Atmos. Chem. Phys.*, *10*(13), 6151–6167, doi:10.5194/acp-10-6151-2010.

Gourdji, S. M., et al. (2012), North American CO_2 exchange: Inter-comparison of modeled estimates with results from a fine-scale atmospheric inversion, *Biogeosciences*, *9*(1), 457–475, doi:10.5194/bg-9-457-2012.

Guanter, L., et al. (2014), Global and time-resolved monitoring of crop photosynthesis with chlorophyll fluorescence, *Proc. Natl. Acad. Sci. U.S.A.*, *111*(14), E1327–E1333, doi:10.1073/pnas.1320008111.

Heimann, M., and M. Reichstein (2008), Terrestrial ecosystem carbon dynamics and climate feedbacks, *Nature*, *451*(7176), 289–292, doi:10.1038/nature06591.

Hui, D., Y. Luo, and G. Katul (2003), Partitioning interannual variability in net ecosystem exchange between climatic variability and functional change, *Tree Physiol.*, *23*(7), 433–442, doi:10.1093/treephys/23.7.433.

Huntzinger, D. N., S. M. Gourdji, K. L. Mueller, and A. M. Michalak (2011), A systematic approach for comparing modeled biospheric carbon fluxes across regional scales, *Biogeosciences*, *8*(6), 1579–1593, doi:10.5194/bg-8-1579-2011.

Huntzinger, D. N., et al. (2012), North American Carbon Program (NACP) regional interim synthesis: Terrestrial biospheric model intercomparison, *Ecol. Modell.*, *232*, 144–157, doi:10.1016/j.ecolmodel.2012.02.004.

Huxman, T., K. Snyder, D. Tissue, A. J. Leffler, K. Ogle, W. Pockman, D. Sandquist, D. Potts, and S. Schwinning (2004), Precipitation pulses and carbon fluxes in semiarid and arid ecosystems, *Oecologia*, *141*(2), 254–268, doi:10.1007/s00442-004-1682-4.

Ise, T., and P. R. Moorcroft (2006), The global-scale temperature and moisture dependencies of soil organic carbon decomposition: An analysis using a mechanistic decomposition model, *Biogeochemistry*, *80*(3), 217–231, doi:10.1007/s10533-006-9019-5.

Joiner, J., Y. Yoshida, A. P. Vasilkov, Y. Yoshida, L. A. Corp, and E. M. Middleton (2011), First observations of global and seasonal terrestrial chlorophyll fluorescence from space, *Biogeosciences*, *8*(3), 637–651, doi:10.5194/bg-8-637-2011.

Keeling, C., S. Piper, R. Bacastow, M. Wahlen, T. Whorf, M. Heimann, and H. Meijer (2005), Atmospheric CO_2 and $^{13}CO_2$ exchange with the terrestrial biosphere and oceans from 1978 to 2000: Observations and carbon cycle implications, in *A History of Atmospheric CO_2 and Its Effects on Plants, Animals, and Ecosystems*, edited by I. T. Baldwin et al., pp. 83–113, Springer, New York, doi:10.1007/0-387-27048-5_5.

Krinner, G., N. Viovy, N. de Noblet-Ducoudré, J. Ogée, J. Polcher, P. Friedlingstein, P. Ciais, S. Sitch, and I. C. Prentice (2005), A dynamic global vegetation model for studies of the coupled atmosphere-biosphere system, *Global Biogeochem. Cycles*, *19*, GB1015, doi:10.1029/2003GB002199.

Department of Energy through the Ameriflux Management Project, the Midwestern Center of the National Institute for Global Environmental Change (NIGEC), the National Institute for Climate Change Research (NICCR), the Terrestrial Carbon Program (TCP), and the Terrestrial Ecosystem Sciences (TES) programs. CO_2 measurements at LJA were supported by the Scripps CO_2 program. We thank the following individuals for collecting and providing the atmospheric CO_2 data from the following sites: Arlyn Andrews (NOAA) for SNP, AMT, WBI, BAO, LEF, and WKT; Kirk Thoning (NOAA) for BRW; Matt J. Parker (SRNL) for SCT; Marc Fischer (LBNL) and Arlyn Andrews (NOAA) for WGC; Kenneth Davis, Scott Richardson, and Natasha Miles (Pennsylvania State University) for CVA, OZA, KEW, CEN, MEA, ROL, and GAL; Britton Stephens (NCAR) and the Regional Atmospheric Continuous CO_2 Network in the Rocky Mountains (RACCOON) for NWR, SPL, and HDP, Beverley Law (Oregon State University) and the TERRA-PNW group for data from five Oregon sites; William Munger (Harvard University) and Steven Wofsy (Harvard University) for HFM; Doug Worthy (Environment Canada) for CDL, FRD, SBL, EGB, ETL, LLB, and CHM; Danilo Dragoni (Indiana University) and Kimberly Novick (Indiana University) for MMS; and Ralph Keeling (Scripss Institution of Oceanography) for LJA. Finally, we acknowledge Sharon Gourdji and Kim Mueller for their earlier efforts in collecting and processing those data sets, Vineet Yadav and Yoichi Shiga for their efforts in developing, testing, and improving the Geostatistical Inverse Modeling tools. Users can contact the authors (yyfang@carnegiescience.edu) for accessing the data and method used in this study.

Law, B. E., et al. (2002), Environmental controls over carbon dioxide and water vapor exchange of terrestrial vegetation, *Agric. For. Meteorol.*, *113*, 97–120, doi:10.1016/S0168-1923(02)00104-1.

Lee, J.-E., et al. (2013), Forest productivity and water stress in Amazonia: Observations from GOSAT chlorophyll fluorescence, *Proc. R. Soc. B*, *280*, 20130171, doi:10.1098/rspb.2013.0171.

Lin, J. C., C. Gerbig, S. C. Wofsy, A. E. Andrews, B. C. Daube, K. J. Davis, and C. A. Grainger (2003), A near-field tool for simulating the upstream influence of atmospheric observations: The Stochastic Time-Inverted Lagrangian Transport (STILT) model, *J. Geophys. Res.*, *108*(D16), 4493, doi:10.1029/2002JD003161.

Lloyd, J., and J. Taylor (1994), On the temperature dependence of soil respiration, *Funct. Ecol.*, *8*, 315–323

Matthias, P., Ö. Mats, L. Mikaell Ottosson, I. Ulrik, S. Jörgen, G. Achim, L. Anders, and B. N. Mats (2014), A 12-year record reveals pre-growing season temperature and water table level threshold effects on the net carbon dioxide exchange in a boreal fen, *Environ. Res. Lett.*, *9*(5), 055006, doi:10.1088/1748-9326/9/5/055006.

Mesinger, F., et al. (2006), North American regional reanalysis, *Bull. Am. Meteorol. Soc.*, *87*(3), 343–360, doi:10.1175/BAMS-87-3-343.

Michalak, A. M., L. Bruhwiler, and P. P. Tans (2004), A geostatistical approach to surface flux estimation of atmospheric trace gases, *J. Geophys. Res.*, *109*, D14109, doi:10.1029/2003JD004422.

Mueller, K. L., S. M. Gourdji, and A. M. Michalak (2008), Global monthly averaged CO_2 fluxes recovered using a geostatistical inverse modeling approach: 1. Results using atmospheric measurements, *J. Geophys. Res.*, *113*, D21114, doi:10.1029/2007JD009734.

Mueller, K. L., V. Yadav, P. S. Curtis, C. Vogel, and A. M. Michalak (2010), Attributing the variability of eddy-covariance CO_2 flux measurements across temporal scales using geostatistical regression for a mixed northern hardwood forest, *Global Biogeochem. Cycles*, *24*, GB3023, doi:10.1029/2009GB003642.

Parazoo, N. C., K. Bowman, J. B. Fisher, C. Frankenberg, D. B. A. Jones, A. Cescatti, Ó. Pérez-Priego, G. Wohlfahrt, and L. Montagnani (2014), Terrestrial gross primary production inferred from satellite fluorescence and vegetation models, *Global Change Biol.*, *20*(10), 3103–3121, doi:10.1111/gcb.12652.

Peters, W., et al. (2007), An atmospheric perspective on North American carbon dioxide exchange: CarbonTracker, *Proc. Natl. Acad. Sci. U.S.A.*, *104*(48), 18,925–18,930, doi:10.1073/pnas.0708986104.

Piao, S., et al. (2013), Evaluation of terrestrial carbon cycle models for their response to climate variability and to CO_2 trends, *Global Change Biol.*, *19*(7), 2117–2132, doi:10.1111/gcb.12187.

Richardson, A. D., et al. (2012), Terrestrial biosphere models need better representation of vegetation phenology: Results from the North American Carbon Program Site Synthesis, *Global Change Biol.*, *18*(2), 566–584, doi:10.1111/j.1365-2486.2011.02562.x.

Richardson, S. J., N. L. Miles, K. J. Davis, E. R. Crosson, C. W. Rella, and A. E. Andrews (2011), Field testing of cavity ring-down spectroscopy analyzers measuring carbon dioxide and water vapor, *J. Atmos. Oceanic Technol.*, *29*(3), 397–406, doi:10.1175/JTECH-D-11-00063.1.

Rigge, M., B. Wylie, L. Zhang, and S. P. Boyte (2013), Influence of management and precipitation on carbon fluxes in great plains grasslands, *Ecol. Indic.*, *34*, 590–599, doi:10.1016/j.ecolind.2013.06.028.

Schaefer, K., et al. (2012), A model-data comparison of gross primary productivity: Results from the North American Carbon Program site synthesis, *J. Geophys. Res.*, *117*, G03010, doi:10.1029/2012JG001960.

Schmid, H. P., C. S. B. Grimmond, F. Cropley, B. Offerle, and H.-B. Su (2000), Measurements of CO_2 and energy fluxes over a mixed hardwood forest in the mid-western United States, *Agric. For. Meteorol.*, *103*(4), 357–374, doi:10.1016/S0168-1923(00)00140-4.

Schneising, O., M. Reuter, M. Buchwitz, J. Heymann, H. Bovensmann, and J. P. Burrows (2014), Terrestrial carbon sink observed from space: Variation of growth rates and seasonal cycle amplitudes in response to interannual surface temperature variability, *Atmos. Chem. Phys.*, *14*(1), 133–141, doi:10.5194/acp-14-133-2014.

Schwalm, C. R., et al. (2010), A model-data intercomparison of CO_2 exchange across North America: Results from the North American Carbon Program site synthesis, *J. Geophys. Res.*, *115*, G00H05, doi:10.1029/2009JG001229.

Shiga, Y. P., A. M. Michalak, S. M. Gourdji, K. L. Mueller, and V. Yadav (2014), Detecting fossil fuel emissions patterns from subcontinental regions using North American in situ CO_2 measurements, *Geophys. Res. Lett.*, *41*, 4381–4388, doi:10.1002/2014GL059684.

Skamarock, W. C., and J. B. Klemp (2008), A time-split nonhydrostatic atmospheric model for weather research and forecasting applications, *J. Comput. Phys.*, *227*(7), 3465–3485, doi:10.1016/j.jcp.2007.01.037.

Stephens, B. B., N. L. Miles, S. J. Richardson, A. S. Watt, and K. J. Davis (2011), Atmospheric CO_2 monitoring with single-cell NDIR-based analyzers, *Atmos. Meas. Tech.*, *4*(12), 2737–2748, doi:10.5194/amt-4-2737-2011.

Thoning, K. W., D. R. Kitzis, and A. Crotwell (2014), *Atmospheric Carbon Dioxide Dry Air Mole Fractions From Quasi-Continuous Measurements at Barrow, Alaska*, Natl. Clim. Data Cent., NESDIS, NOAA, U.S. Dep. of Commer., Boulder, Colo., doi:10.7289/V5RR1W6B.

Urbanski, S., C. Barford, S. Wofsy, C. Kucharik, E. Pyle, J. Budney, K. McKain, D. Fitzjarrald, M. Czikowsky, and J. W. Munger (2007), Factors controlling CO_2 exchange on timescales from hourly to decadal at Harvard Forest, *J. Geophys. Res.*, *112*, G02020, doi:10.1029/2006JG000293.

van der Werf, G. R., J. T. Randerson, L. Giglio, G. J. Collatz, P. S. Kasibhatla, and A. F. Arellano Jr. (2006), Interannual variability in global biomass burning emissions from 1997 to 2004, *Atmos. Chem. Phys.*, *6*(11), 3423–3441, doi:10.5194/acp-6-3423-2006.

Vargas, R., D. D. Baldocchi, J. I. Querejeta, P. S. Curtis, N. J. Hasselquist, I. A. Janssens, M. F. Allen, and L. Montagnani (2010), Ecosystem CO_2 fluxes of arbuscular and ectomycorrhizal dominated vegetation types are differentially influenced by precipitation and temperature, *New Phytol.*, *185*(1), 226–236, doi:10.1111/j.1469-8137.2009.03040.x.

Wang, J., et al. (2014), Comparison of gross primary productivity derived from GIMMS NDVI3g, GIMMS, and MODIS in Southeast Asia, *Remote Sens.*, 6(*3*), 2108–2133, doi:10.3390/rs6032108.

Wang, W., P. Ciais, R. R. Nemani, J. G. Canadell, S. Piao, S. Sitch, M. A. White, H. Hashimoto, C. Milesi, and R. B. Myneni (2013), Variations in atmospheric CO_2 growth rates coupled with tropical temperature, *Proc. Natl. Acad. Sci. U.S.A.*, *110*(32), 13,061–13,066, doi:10.1073/pnas.1219683110.

Wang, X., et al. (2014), A two-fold increase of carbon cycle sensitivity to tropical temperature variations, *Nature*, *506*(7487), 212–215, doi:10.1038/nature12915.

Yadav, V., K. L. Mueller, D. Dragoni, and A. M. Michalak (2010), A geostatistical synthesis study of factors affecting gross primary productivity in various ecosystems of North America, *Biogeosciences*, *7*(9), 2655–2671, doi:10.5194/bg-7-2655-2010.

Yi, C., et al. (2010), Climate control of terrestrial carbon exchange across biomes and continents, *Environ. Res. Lett.*, *5*(3), 034007.

Yu, G.-R., et al. (2013), Spatial patterns and climate drivers of carbon fluxes in terrestrial ecosystems of China, *Global Change Biol.*, *19*(3), 798–810, doi:10.1111/gcb.12079.

Zeng, N., A. Mariotti, and P. Wetzel (2005), Terrestrial mechanisms of interannual CO_2 variability, *Global Biogeochem. Cycles*, *19*, GB1016, doi:10.1029/2004GB002273.